Journal of Fluids and Structures 17 (2003) 491–510

JOURNAL OF FLUIDS AND STRUCTURES

www.elsevier.nl/locate/jnlabr/yjfls

Energetics of axisymmetric fluid-filled pipes up to high frequencies

A. Bocquillet, M.N. Ichchou*, L. Jezequel

Laboratoire de Tribologie et Dynamique des Systèmes, Département de Mécanique des Solides, Génie Mécanique et Génie Civil École Centrale de Lyon, 36, Avenue Guy de Collongue, BP 163, 69131 Écully, France

Received 6 March 2001; accepted 8 November 2002

Abstract

The energetics of motions of axisymmetric fluid-filled pipes are presented in this paper, in view of high-frequency modelling. This study deals in particular with derivations of local energy equations well suited for the prediction of averaged response of coupled fluid–structure systems. The derivation of the latter requires special manipulation of the kinematic dynamics based here on the notion of propagation modes. Thus, the focus is on the Donnell–Mushtari cylindrical shell with an internal acoustic fluid, a typical example of waveguides with multiple transmission mechanisms. ''Exact'' and statistical approaches are developed for this system. A state-space representation is first proposed; it allows the characterization of propagating modes in a general manner. This propagating content then leads to the formulation of the local energy approach for this canonical problem.

1. Introduction

Vibrational and acoustical energy are usually driven by thin-walled waveguides such as pipes. In fact, many engineering problems involve fluid-filled pipes as components. The latter form a privileged vibration and noise transmission path whose importance may be quantified by predicting the vibrational energy over a wide frequency range. This will ensure appropriate design of pipework towards achieving damage and failure limitation and enhanced noise reduction. Nevertheless, only approaches well suited to the low-frequency range are extensively used in the literature and there is still a need to improve the predictive ability of the transmission mechanism of fluid-filled pipes in the high-frequency domain.

The high-frequency behavior of complex structures is still a subject of active research and interest. Many developments are in progress in order to provide predictive tools well suited to medium and high frequencies and taking into account the numerous features of this domain. Certain peculiarities make the use of classical methods (finite element, boundary element, etc.) ill suited in the nonmodal range. Notably, deterministic approaches often prove to be unusable in the high-frequency range. The existence of uncertainties in the geometric or material properties of the mechanical systems, for instance, involves a statistical point of view mainly when the frequency is high enough.

Among statistical alternatives proposed in the literature for the analysis of the high-frequency domain, let us mention the well-known *Statistical Energy Analysis* (Lyon, 1975; Keane and Price, 1997; Fahy, 1994) as well as a class of *Local* alternatives, that we shall refer to as ''local energy approach'' (Wohlever and Bernhard, 1992; Bouthier and Bernhard, 1995a, b; Ichchou and Jezequel, 1996; Langley, 1995; Carcaterra and Sestieri, 1995; Ichchou et al., 1997). Such alternatives are considered in this paper.

*Corresponding author.
E-mail address: ichchou@mecasola.ec-lyon.fr (M.N. Ichchou).

0889-9746/03/$ - see front matter
doi:10.1016/S0889-9746(02)00161-5

Statistical Energy Analysis (Lyon, 1975; Keane and Price, 1997) (SEA) has become a standard "predictive" tool for high-frequency dynamics. SEA is a quick method which requires a set of global parameters of the studied problem. Moreover, it is energy based, offering a unified treatment for a wide range of engineering problems. From a global energy balance, SEA gives an averaged vibrational energy of each subsystem of complex structures. To authors' knowledge, only a few papers giving a SEA description of fluid-filled pipes can be found in the available literature. In our opinion, the main contributions to this kind of subject were provided by Finnveden (1997a, b), Heckl (1962), Fuller and Fahy (1982), Pavic (1990) and Langley (1994a, b). A SEA model requires the provision of a set of global parameters. This is the main goal of the contributions found in the literature. Indeed, existing papers are concerned with the determination of modal densities, internal and coupling loss factors and power inputs to the fluid-filled pipe problems. For instance, in Heckl (1962) an approximation of modal density for cylinders is given. Langley (1994a, b) reconsidered the same problem using a Donnell–Mushtari cylindrical shell theory (Markus, 1988) and also supplied some results for a curved panel case.

An important contribution to the subject which is directly related to the work we are proposing was made by Finnveden (1997a, b). Finnveden proposed the so-called Spectral Finite Element Method, whose objectives are very close to what the authors call the "Propagative Approach" (Bocquillet, 2000; Houillon, 1999). In fact, both approaches intend to give the dispersion curves of typical dynamical systems and related forced responses. Finnveden presented some applications of this approach for extended "stiffened" plates (Orenius and Finnveden, 1996) and for pipework (Finnveden, 1997a). A number of applications are given in Houillon (1999) for hollow structures and in Bocquillet (2000) for elastoacoustic and periodic structures. This propagative approach is a promising technique which is well suited for medium- and high-frequency modelling (as will be shown in this contribution).

In fact, SEA still requires some improvements (Keane and Price, 1997; Fahy, 1994). On this topic, the reader can find clarifications from references mainly by Fahy (1994), who gives a review of the Statistical Energy Analysis. An interesting survey and a number of critical comments are given. Beyond these studies, a number of works attempt to enhance the accuracy and predictivity of SEA. Among them, we should mention the earlier work of Belov et al. (1977) and the interesting investigations of Nefske and Sung (1987) who proposed the use of the heat conduction analogy to obtain not only the total energy available in SEA, but also the spatial spread of energy density within the subsystems. This leads to an energy formulation of the dynamical equation of motion, instead of the classical formulation based on the displacement field. Basically, this approach can be viewed as a *local energy* formalism whereas the SEA formalism is based on global energies of finite subsystems. This model has been improved by Bernhard and his team (Wohlever and Bernhard, 1992; Bouthier and Bernhard, 1995a, b) and is also discussed in Lase et al. (1996) and Ichchou and Jezequel (1996).

In this paper, the proposed work investigates the energy aspects of a canonical axisymmetrical fluid–structure problem. For this purpose, the basis of the preliminary principle of the propagative approach will be given first. Some fundamental properties related to the spectral problem are then discussed. This leads to an analysis of free waves whose features and characteristics provide a better analysis of energy behavior. Notably, from a state-space formulation of the problem, the propagating behavior of complex elastoacoustic cases are studied. Comparisons with analytical computations, mainly done by Fuller and Fahy (1982), are proposed and a good degree of agreement is noted. The propagating content, when used according to a number of assumptions discussed in the paper, leads to a relevant representation of energy exchanges between propagating modes and to the energy spread within "subsystems". Indeed, that input allows a local energy approach to be formulated. A water-filled pipe is considered in this study as an illustrative example. Comparative results are given in order to show the accuracy of the proposed methodology. In particular the effects of *wave complexity* on the energy models are discussed and numerically checked.

2. State-space formulation of the elastoacoustic problem

The problem considered here is a basic elastoacoustic case (Fig. 1). It consists of a cylindrical shell with an internal acoustic fluid. The shell obeys the Donnell–Mushtari theory (Markus, 1988), and the linearized Helmholtz equation characterizes fluid behavior. In the following subsections, a state-space formulation is summarized and the propagation of the elastoacoustic problem is discussed.

2.1. Structural shell dynamics

Let us consider at first the structural model of the pipe. In the context of this paper, the pipe is represented by a Donnell–Mushtari cylindrical shell (see Fig. 1).

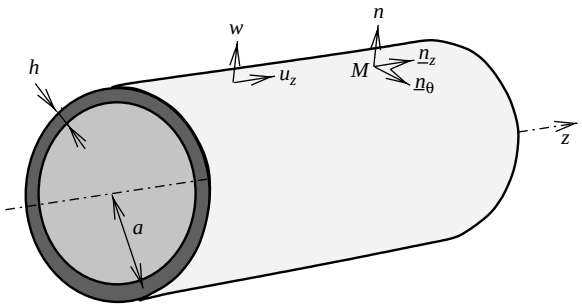

Fig. 1. A Donnell–Mushtari cylindrical shell.

The thickness and the radius of the studied cylindrical shell are, respectively, h, a. Young's modulus, Poisson ratio and the mass density of the material are, respectively, E, ν and ρ. In what follows, u_z, w represent the axial and the radial motion of the shell, and ϕ will be associated with the radial motion w. The normal, radial resulting forces as well as bending moment are respectively N_z, T and M_z. For axisymmetric dynamics, the functional associated with the undamped Donnell–Mushtari cylindrical shell theory can be found as (Dhatt and Batoz, 1992; Markus, 1988):

$$\mathscr{F}^{(s)} = \frac{2\pi a}{4}\int_z \left\{ D\frac{\mathrm{d}\phi}{\mathrm{d}z}\frac{\mathrm{d}\phi^*}{\mathrm{d}z} + C\left(\frac{\mathrm{d}u_z}{\mathrm{d}z} + \nu\frac{w}{a}\right)\frac{\mathrm{d}u_z^*}{\mathrm{d}z} + C\left(\nu\frac{\mathrm{d}u_z}{\mathrm{d}z} + \frac{w}{a}\right)\frac{w^*}{a} - \rho h\omega^2(u_z u_z^* + w w^*) + T^*\left(\phi - \frac{\mathrm{d}w}{\mathrm{d}z}\right) + T\left(\phi^* - \frac{\mathrm{d}w^*}{\mathrm{d}z}\right)\right\}\mathrm{d}z, \tag{1}$$

where $C = Eh/(1-\nu^2)$ and $D = Eh^3/12(1-\nu^2)$. The time dependency of motion is assumed to be $\mathrm{e}^{\mathrm{i}}\omega t$. The superscript s in all follows designates variables linked to the structure. The equation of motion can thus be formulated using the structural functional given in Eq. (1). In fact, the stationarity of such a functional for any variation of kinematic components, leads to a simple form of Euler equations which can be expressed in the following format (Bocquillet, 2000):

$$\mathbb{J}_a^{(s)} \times \frac{\mathrm{d}}{\mathrm{d}z}\mathbf{Y}^{(s)} = \mathbb{H}^{(s)}\mathbf{Y}^{(s)}. \tag{2}$$

$\mathbb{J}_a^{(s)}$ as well as the state-space vector $\mathbf{Y}^{(s)}$ and matrix $\mathbb{H}^{(s)}$ are given in Appendix A. $\mathbb{J}_a^{(s)}$ is a symplectic 6×6 matrix and $\mathbb{H}^{(s)}$ is found to be symmetrical. This symmetry establishes the main mathematical properties of the state-space equation (Yakubovitch and Starzhinskii, 1975). The latter is a simple presentation of the equations of motion, and it can be compared to the expression given by Wang and Norris (1995).

2.2. Fluid–structure functional

The bounded internal acoustic fluid inside the pipe (volume Ω) is governed by the linear Helmholtz equation. Considering $\partial\Omega$ as the internal boundary of the bounded fluid and denoting $\mathbf{n}$ as its unit normal, this gives

$$\begin{aligned} &\Delta \mathrm{p} + k^2 \mathrm{p} = 0 \quad \text{in } \Omega, \\ &\frac{\partial \mathrm{p}}{\partial \mathbf{n}} = \rho_f \omega^2 w \quad \text{on } \partial\Omega, \end{aligned} \tag{3}$$

with $k = \omega/c$, a real value. The functional associated with the first equation and the coupling between the two media, namely Eq. (3) are introduced by

$$\mathscr{F}^{(a)} = \frac{1}{4}\int_\Omega ({}^t\nabla p^* \nabla p - \mathbf{k}^2 \mathrm{p}^* \mathrm{p})\,\mathrm{d}\Omega, \tag{4}$$

and

$$\mathscr{F}^{(s,a)} = -\frac{1}{2}\int_{\partial\Omega}^{t} (w^* \mathrm{p} + w \mathrm{p}^*)\,\mathrm{d}(\partial\Omega). \tag{5}$$

The superscript a (resp. s, a) designates acoustic (resp. structural acoustic) contributions. Finally, the functional of the coupled fluid structure problem considered here can be summarized as follows:

$$\mathscr{F} = \mathscr{F}^{(a)} + \mathscr{F}^{(s)} + \mathscr{F}^{(s,a)}. \tag{6}$$

The state-space formulation for the coupled fluid structure problem needs to be considered now. To do so, we will use a particular approximation of the acoustic field.

2.3. State-space formulation for the coupled problem

In the high-frequency range, the nonplanar dynamics in the fluid has to be taken into account. The acoustic pressure field $\mathrm{p}(r,\theta,z)$ is approximated by using suitable decomposition functions. A separation of variables is proposed by Finnveden (1997b), who used a finite element discretization with polynomials of high degree for the fluid section. Here, a decomposition of the pressure field using cylindrical Bessel functions is proposed. Indeed, for the fluid axisymmetric motion, an appropriate approximation of the acoustic internal field can be shown to be

$$\mathrm{p}(r,\theta,z)=\sum_{j=1}^{m}\frac{\mathrm{J}_0(\vartheta_j\, r/a)}{\sqrt{\pi}\mathrm{J}_0(\vartheta_j)}p_j(z). \tag{7}$$

As the analysis is limited to the axisymmetric motion, ϑ_j designates the jth root of the first-order Bessel function of the first kind ($\mathrm{J}_1(\vartheta_j)=0$). It should be noted that the orthogonal Bessel function properties secure convergence of the given approximation. Using the given decomposition with combination of the coupled functional of problem (6), one can readily obtain the following state-space formulation for the coupled elastoacoustic problem:

$$\mathbb{J}_a^{(c)}\frac{\mathrm{d}}{\mathrm{d}z}\mathbf{Y}^{(c)}=\mathbb{H}^{(c)}\mathbf{Y}^{(c)}. \tag{8}$$

The expressions of $\mathbb{J}_a^{(c)}$ as well as the state-space vector $\mathbf{Y}^{(c)}$ and matrix $\mathbb{H}^{(c)}$ are given in Appendix A. In the following, n will be identified with the intrinsic size of matrixes, namely $(m+3)$. The state-space formulation for the coupled elastoacoustic problem is now established. The propagation for dissipative waveguides is also possible. In this case $\mathbb{H}^{(c)}$ becomes complex symmetrical.

3. Propagative approach based on state-space equation

The state-space representation for any complex elastoacoustic problem can be written as explained above. This leads to a set of first-order differential equations, where the independent variable z is real. In the matrix notation, this system becomes a single vector-differential equation (9). In the following, the fundamental solutions of the state-space equations are examined.

3.1. Existence and uniqueness—Matrizant

The matrix format of the set of first-order differential equation written for any elastoacoustic configuration takes the following general form:

$$\mathbb{J}_a\frac{\mathrm{d}}{\mathrm{d}z}\mathbf{Y}=\mathbb{H}\mathbf{Y}, \tag{9}$$

with $\mathbb{H}$ a complex symmetrical matrix and $\mathbf{Y}$ the state-space vector. The matrix $\mathbb{J}_a$ is a $2n\times 2n$ matrix whose general expression is given by

$$\mathbb{J}_a=\begin{pmatrix}0 & -\mathbb{I}_n\\ \mathbb{I}_n & 0\end{pmatrix}. \tag{10}$$

This matrix obeys some interesting formulae (for instance, $\mathbb{J}_a^2=-\mathbb{I}_{2n}\ldots$). The matrizant $\mathbb{Z}$ is a matrix whose columns are fundamental solutions, which are linearly independent, of the state-space equation (9). These fundamental solutions are chosen so that $\mathbb{Z}(0)=\mathbb{I}$ [see for instance Yakubovitch and Starzhinskii (1975)]. Coefficients of the state-space matrix are generally complex-valued, integrable, piecewise-continuous functions in any finite interval of z. In fact, the mechanical characteristics of the problem are bounded, piecewise-continuous and integrable. The decomposition functions used in the state-space equation procedure (7) are generally piecewise-continuous and continuously differentiable in Ω (often piecewise $\mathscr{C}^1$). Those functions as well as their simultaneous derivatives are assumed to be integrable in Ω. Coefficients of $\mathbb{H}$ are thus integrable, piecewise-continuous. Thus, in the class of continuous vector-functions with integrable piecewise-continuous derivative, it can be shown that the matrix $\mathbb{Z}$ exists and is unique. An outline of the proof of the existence and uniqueness of the solution is given in Yakubovitch and Starzhinskii (1975).

Each column of the matrizant $\mathbb{Z}$ defines an independent solution such as

$$\forall z \quad \det(\mathbb{Z}(z)) \neq 0. \tag{11}$$

In this case, any solution $\mathbf{Y}(z)$ of the state-space equation (9) may be expressed in terms of a fundamental set as

$$\mathbf{Y}(z) = \mathbb{Z}(z)\varphi, \tag{12}$$

where φ characterizes the contribution of each fundamental-independent solution. In the particular case of Hamiltonian systems, the state-space matrix $\mathbb{H}$ being real symmetrical induces an orthogonality relationship, such as

$${}^{t}\mathbb{Z}\mathbb{J}_a\mathbb{Z} = \mathbb{J}_a. \tag{13}$$

In this case, the matrizant $\mathbb{Z}$ is said to be $\mathbb{J}$-orthogonal, or equivalently, that $\mathbb{Z}$ verifies a symplectic orthogonality.

3.2. Definition of propagative modes

The matrizant of the state-space equation (9) can be obtained from different procedures. In the situation of a constant (with respect to z) state-space matrix $\mathbb{H}$ (a condition that is met in nearly all practical structures with constant characteristics), the matrizant of Eq. (9) can be shown to be (Pease, 1978):

$$\mathbb{Z}(z) = \mathrm{e}^{-\mathbb{J}_a\mathbb{H}z}. \tag{14}$$

The concept of propagative modes then appears naturally. In fact, the set of fundamental solutions of the given first-order matrix equation can be obtained by solving an eigenvalue problem. Indeed, propagative modes result from the spectrum of the matrix $-\mathbb{J}_a\mathbb{H}$. Hence, if an eigenvalue and an associated eigenvector are given by $(-\mathrm{i}k_j, \mathbf{V}_j)$, then the state-space vector solution of Eq. (9) will be given by

$$\mathbf{Y}_j(z) = \mathbf{V}_j\mathrm{e}^{-\mathrm{i}k_j z}. \tag{15}$$

It can readily be verified that the given vector satisfies the differential equation (9), k_j being the wavenumber of the jth propagation mode ($k_j \in \mathbb{C}$). The general state-space vector can therefore be written using the new set of fundamental solutions as

$$\mathbf{Y}(z) = \sum_{j=1}^{2n} \mathbf{V}_j\mu_j(z) = \mathbb{V}\mu(z). \tag{16}$$

The vector μ is called here the *wave vector*, and $\mathbb{V}$ is the square matrix with columns $\mathbf{V}_j$. Moreover, it can readily be established that both $\mathrm{i}k_j$ and $-\mathrm{i}k_j$ are eigenvalues. This important result proves the reciprocity of propagation in the case of Hamiltonian systems. The outline of the proof uses the property of $\mathbb{J}$-orthogonality of the matrizant $\mathbb{Z}$. In the following, the nth first eigenvalues and eigenvectors are associated with the propagation towards positive z (negative imaginary part of k_j, $\lambda_j = \mathrm{e}^{-\mathrm{i}k_j z}$), the next n eigenvectors are associated with λ_{n+j} ($\lambda_{n+j} = 1/\lambda_j$). This is the standard notation used in this text. In what follows, matrixes $\mathbb{D}(z)$ and $\mathbb{D}^+(z)$ are diagonal matrixes such as

$$\mathbb{D}(z) = (\mathrm{e}^{-\mathrm{i}k_j z})_{j=1:2n, j=1:2n}, \quad \mathbb{D}^+(z) = (\mathrm{e}^{-\mathrm{i}k_j z})_{j=1:n, j=1:n}. \tag{17}$$

Ultimately, it should be mentioned that properties of such a representation are of fundamental interest in terms of understanding energy behavior. The main properties are discussed in what follows.

3.3. Propagation relationships for a complex waveguide

When dealing with energy propagation inside a complex propagator, the energy transfer between two given sections at z and z' for instance may be quantified. In terms of propagative modes, this transfer expression can be easily written using the new variable μ instead of $\mathbf{Y}$. Indeed

$$\mathbf{Y}(z) = \mathbb{V}\mu(z), \quad \mu(z') = \mathbb{D}(z' - z)\mu(z). \tag{18}$$

Hence, the transfer expression between z and z' can be represented by

$$\mathbf{Y}(z') = \mathbb{V}\mathbb{D}(z' - z)\mathbb{V}^{-1}\mathbf{Y}(z). \tag{19}$$

This expression allows the state-space vector $\mathbf{Y}$ to be known at any place in the systems if we know its value at a given position and the eigenparameters of the state-space equation.

3.4. Orthogonality relationships

For Hamiltonian conservative systems the matrix $\mathbb{H}$ is real symmetrical. Two different eigensolutions $\mathbf{V}_l$ and $\mathbf{V}_j$ for the given system obey the general orthogonality property:

$$(k_l^* - k_j)^t \mathbf{V}_l^* \mathbb{J}_a \mathbf{V}_j = 0. \tag{20}$$

For nonHamiltonian dissipative systems ($\mathbb{H}$ is complex symmetric) a different orthogonality law can be formulated:

$$(k_l + k_j)^t \mathbf{V}_l \mathbb{J}_a \mathbf{V}_j = 0. \tag{21}$$

In practice, this orthogonality law can be used in order to plot dispersion curves (real and imaginary parts of wavenumbers k_j versus frequency). In fact, eigenvectors often evolve unceasingly with frequency. Orthogonality enables a concise analysis of propagation modes. Specifically, in the dispersion curves characterization below, the following criterion (quadratic cost variable to be maximized) will be used:

$$^t \mathbf{V}_l \mathbb{J}_a \mathbf{V}_j. \tag{22}$$

In this expression $\mathbf{V}_l$ and $\mathbf{V}_j$ are normalized eigenvectors. As mentioned above, the spectral problem must be solved at chosen frequencies. Let us denote the set of ordered frequencies by $(\omega_r)_{r=1\ldots}$ with $(\omega_{r-1} < \omega_r)$ in view of dispersion curve representation. Suppose that the qth propagation mode is being considered, namely $\mathbf{V}_q$. If $\mathbf{V}_q(\omega_{(r-1)})$ is the qth propagation mode at the step $r-1$, the propagation mode $\mathbf{V}_q(\omega_r)$ at the step r has to be defined among a set of eigensolutions. A maximum value of the criterion $^t\mathbf{V}_q(\omega_{r-1})\mathbb{J}_a\mathbf{V}_j(\omega_r)$ allows a definition of this eigensolution at the next frequency step. This results in a practical numerical way for plotting dispersion curves.

4. Numerical results for the fluid-filled pipe

A complete theoretical analysis of dispersion curves for structural shells coupled with internal fluid, was done by Kumar (1972) and Kumar and Stephens (1972). In this study, the radial dependency of structural response was chosen (their theoretical expressions use Bessel functions). Dispersion curves were thus plotted in the axisymmetric coupled configuration. In another work, Sinha et al. (1992) limited the analysis to real wavenumbers and added the external radiating behavior. Here, dispersion curves for the elastoacoustic case will be given from spectral analysis of the state-space equation.

Indeed, according to the analysis of the previous section, fundamental solutions of Eq. (8) are exponential dependent. The generalized eigenvalue problem form of

$$-\mathrm{i}k_j \mathbb{J}_a^{(c)} \mathbf{V}_j^{(c)} = \mathbb{H}^{(c)} \mathbf{V}_j^{(c)} \tag{23}$$

provides the wavenumbers k_j and associated propagation modes $\mathbf{V}_j^{(c)}$. This determination of propagation is a numerical alternative to nonlinear approaches used by Fuller and Fahy (1982). Dispersion curves are given in the case of a steel shell filled with water. The mechanical/geometrical characteristics of the system are summarized in Table 1.

Here ϖ is the nondimensional frequency $\varpi = \omega a/c_s$, where $c_s = \sqrt{E/\rho_s/(1-\nu^2)}$ corresponds to the extensional phase speed of the shell material. It should be noted that convergence is reached with a small number of approximation functions for the pressure field. Fig. 2 gives the real and imaginary parts of the wavenumbers extracted from the state-space formulation obtained in the damped case. For extended comments of the dispersion curves, we can refer to Fuller and Fahy (1982). In the low-frequency range, the first branch corresponds to a fluid mode. When frequency increases, coupling effects take place, involving radial displacement. At the beginning, the second branch is essentially a dilatational mode. In the frequency interval $\varpi \in [0, 2.5]$, up to 5 modes can propagate far from the discontinuities in each direction.

Table 1
Physical characteristics

	h/a	ρ (kg/m^3)	ρ_f (kg/m^3)	c (m/s)	E (N/m^2)	ν	η
Shell	0.05	7800	—	—	19.2×10^3	—	0.01
Water	—	—	1000	1500	—	—	—

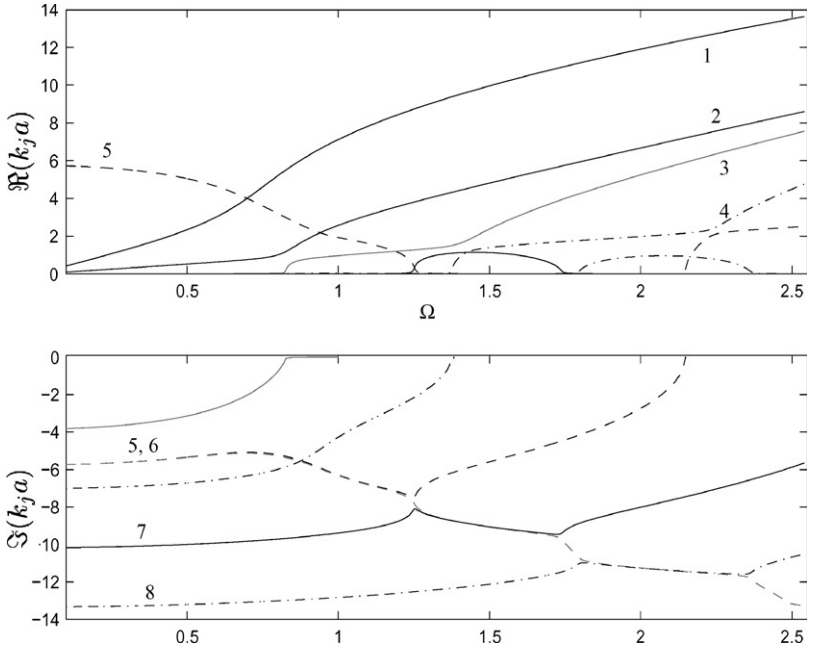

Fig. 2. Dispersion curve (real and imaginary parts) for the Donnell–Mushtari cylindrical shell coupled with an internal fluid.

5. Local energy approach formulation

In this section, the local energy approach associated with the propagation mode description will be presented in depth. As an illustration, the canonical fluid-filled pipe considered in this paper will be numerically explained. The energy formulation uses the propagation modes extracted from the previous section and requires a set of simplifications mainly linked to the physical behavior of waves at high frequencies. Therefore, exploitation of the propagative approach to derive energy quantities is first analyzed. The interest of such a representation of dynamical behavior is also presented in regard to some matrix properties. Ultimately, the local energy model is derived, providing a kind of generalization of some results found in the literature (Wohlever and Bernhard, 1992; Ichchou et al., 1997).

5.1. Kinematic analysis from the propagative approach

The propagative approach explained in the previous section provides a set of $\mathbb{J}$-orthogonal propagation modes (13). They form a new basis for the dynamic motion of the elastoacoustic problem. In fact, as established above, the state vector can be expressed as a linear superposition of the given propagation modes:

$$\mathbf{Y}^{(c)}(z) = \mathbb{V}\mu(z), \tag{24}$$

$\mathbb{V}$ being the matrix of $2n$ solutions computed from Eq. (23). Indeed, the computation of the kinematic solution can be provided using the change of variables (24) and a set of suitable boundary conditions. In the context of this paper, the problem represented in Fig. 3 will be completely analyzed. For this canonical problem, the acoustic boundary conditions written in terms of the state-space vector components are as follows (with $K_d = -M_p\,\omega^2 + \mathrm{i}C_p\omega + K_p$):

$$f_j^{(a)}(0) = -\frac{\mathrm{i}\sqrt{\pi}a^2}{\omega} v_{ex}\,\delta_1(j),$$

$$f_j^{(a)}(L) = -\frac{\pi\sqrt{\pi}a^4}{K_d} p_1(L)\delta_1(j), \tag{25}$$

where the $f^{(a)}$ expression is given in Appendix A (Eq. (A.5)), and $(\delta_1(j) = 0$ if $j \neq 1)$. The pressure field inside the bounded domain Ω, obeys expression (7).

Following the classification of the eigenvalues proposed above, the wave vector $\mu(z)$ can be divided into right-propagating wave vector μ_R and left-propagating wave vector μ_L, as shown in Fig. 4. The boundary conditions can thus

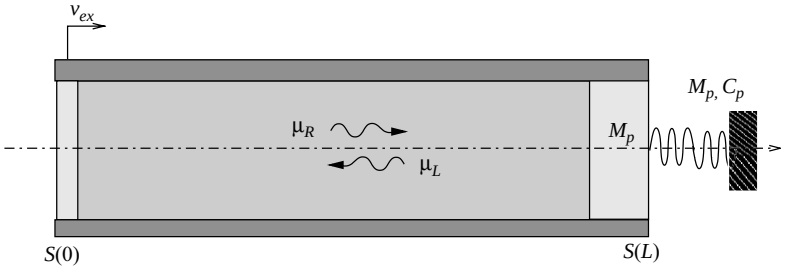

Fig. 3. Pipe excited on $z = 0$ with a mass/spring–damper system on $z = L$.

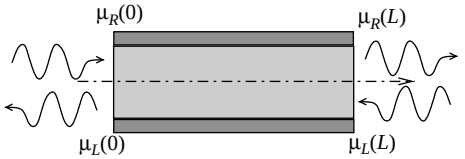

Fig. 4. Wave transport between two singularities.

be written in terms of waves as follows:

$$\mu_R(0) = \mathbb{C}^{(1)}\mu_L(0) + \mu_{ex}, \quad \mu_L(L) = \mathbb{C}^{(2)}\mu_R(L), \tag{26}$$

where μ_{ex} is the incident wave associated with the imposed speed at $z = 0$. Expression (26) corresponds to the reflections of both ends, where $\mathbb{C}^{(1)}$ and $\mathbb{C}^{(2)}$ are the generalized reflection matrixes. To complete the wave analysis of the given problem, the wave transport phenomenon must be introduced. The relation between the wave vector at any section and the boundaries is given by Yong and Lin (1989) as follows:

$$\mu(z) = \begin{pmatrix} \mathbb{D}^+(z) & 0 \\ 0 & \mathbb{D}^+(L-z) \end{pmatrix} \begin{pmatrix} \mu_R(0) \\ \mu_L(L) \end{pmatrix}. \tag{27}$$

Expressions (26), (27) provide the solution system of the elastoacoustic problem in terms of wave vectors μ. Reconstruction of the state vector solution is then readily obtained using expression (24).

5.2. Basic energy formulas from the propagating approach

The energy quantities [the kinetic energy density $T_k(z)$, the potential energy density $U_p(z)$ as well as the active energy flow $\Pi(z)$] for an elastoacoustic system are dealt with below. The expression of the active energy flow $\Pi(z)$ in the elastoacoustic waveguide can be computed, in the propagation mode state, as follows (Bocquillet, 2000; Miller and Von Flotow, 1989):

$$\Pi(z) = -\frac{i\omega}{4}\,{}^t\mathbf{Y}^{(c)*}(z)\mathbb{J}_a\mathbf{Y}^{(c)}(z) = {}^t\,\mu^*(z)\mathbb{P}\mu(z) \tag{28}$$

with

$$\mathbb{P} = -\frac{i\omega}{4}\,{}^t\mathbb{V}^*\mathbb{J}_a\mathbb{V}. \tag{29}$$

The resulting energy flow matrix $\mathbb{P}$ is a Hermitian matrix. $\mathbb{P}$ format is dependent on the nature of the system. Coefficients of this energy flow matrix are representative of the contribution of interferences between the set of propagation modes:

$$P_{jl} = -\frac{i\omega}{4}\,{}^t\mathbf{V}_j^*\mathbb{J}_a\mathbf{V}_l. \tag{30}$$

We recall the orthogonality relationships linked to the spectral problem, and obtained in the previous section:

$$(k_j^* - k_l)\,{}^t\mathbf{V}_j^*\mathbb{J}_a\mathbf{V}_l = 0. \tag{31}$$

Hence, some results given by Mead (1973) concerning the energy flow characteristics for simple undamped vibrating periodic systems are also obtained here. In fact, in the particular case of Hamiltonian undamped elastoacoustic problems, Eq. (31) gives evidence of the following.

(a) If j is a pure evanescent wave, (31) shows that $\mathbb{P}_{j,j} = 0$. There is no contribution of evanescent waves to the net energy flow. However, the interference between the incident evanescent wave j and the reflected evanescent wave l with $(k_l^* = -k_j)$ contributes to the net energy flow.
(b) Interference between any evanescent wave and any propagative wave has no contribution to the net energy flow.
(c) A propagative wave j contributes to the energy flow, only for the diagonal term $\mathbb{P}_{j,j}$.

In the case of a dissipative waveguide, the energy flow matrix $\mathbb{P}$ can be expressed as a full matrix. So out-of-diagonal terms contribute to the energy flow at any section of the pipe. The computation of energy densities (kinetic and potential) can also be performed in a similar manner. In fact, it can be readily shown that

$$T_k(z) = {}^t\mu^*(z)\mathbb{K}_\mu\mu(z), \quad U_p(z) = {}^t\mu^*(z)\mathbb{M}_\mu\mu(z). \tag{32}$$

$\mathbb{K}_\mu$ and $\mathbb{M}_\mu$ are the stiffness and mass matrix in the propagation modes space. The analysis and simplifications proposed in the next subsection are mainly based on a discussion on the energy flow matrix format, namely matrix $\mathbb{P}$.

5.3. Energy flow partition at a boundary

Close to a boundary, it is more convenient to separate μ into incident waves (μ_I) and scattered waves (μ_S), so that one can easily define the incident and reflected energy flow at a boundary. Let us at first concentrate our analysis on the boundary located at $z = L$ (see Fig. 5). Indeed, incident and reflected energy flow at this boundary can be defined in the following using bilinear forms:

$$\Pi_I(L) \stackrel{\text{def}}{=} {}^t\mu(L)^*\mathbb{P}_I\mu(L), \quad \Pi_S(L) \stackrel{\text{def}}{=} {}^t\mu(L)^*\mathbb{P}_S\mu(L) \tag{33}$$

with

$$\mathbb{P}_I = \begin{pmatrix} \mathbb{P}_R & \mathbb{P}_{R,L} \\ \mathbb{P}_{L,R} & \mathbb{O} \end{pmatrix}, \quad \mathbb{P}_S = \begin{pmatrix} \mathbb{O} & \mathbb{O} \\ \mathbb{O} & -\mathbb{P}_L \end{pmatrix}, \tag{34}$$

where $\mathbb{P}_{Rij} = \mathbb{P}_{ij}$ and $(i,j = 1:n)$, $\mathbb{P}_{Lij} = \mathbb{P}_{ij}$ and $(i,j = n:2n)$, $\mathbb{P}_{R,Lij} = \mathbb{P}_{ij}$ for $(i = 1:n)$ and $(j = n:2n)$ and $\mathbb{P}_{L,R} = {}^t\mathbb{P}^*_{R,L}$.

This is a somewhat arbitrary partition of the net energy flow at the interface, which ensures that

(a) the causality principle will be respected, i.e., the reflected energy flow will be smaller than the incident energy;
(b) the energy balance will be respected, i.e., the net energy flow $\Pi(L)$ will be equal to $(\Pi_I(L) - \Pi_S(L))$.

It should be mentioned that the matrix $\mathbb{P}_{R,L}$ corresponds to the coherent energy flow. $\mathbb{P}_R$ and $\mathbb{P}_L$ represent, respectively, the participation of incident and reflected waves. Properties of these interferences and contributions of their interactions to the energy propagation can lead to very interesting simplifications, mainly at high frequencies.

5.4. Statistics and local energy variables at a boundary

In fact, phase fluctuations of the waves μ_j can be related to variations of frequency, uncertainties of guide length, Young's modulus and so on. Due to relation (27) the phase difference between two different propagating waves varies

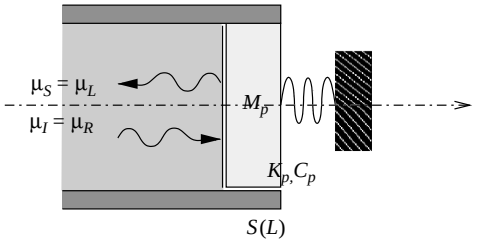

Fig. 5. Scattering of propagation modes μ_{R_j} on the boundary $S(L)$.

far from discontinuities. Between two incident waves on one singularity, the propagation from the opposite boundary ensures that their interference contribution $\mathbb{P}_{i,j}\mu_{I_i}^*(L)\mu_{I_j}(L)$ to energy flow balances are neglected. *Incident waves are thus assumed to be uncorrelated*. In addition, the reflection coefficients do not always induce enough phase fluctuations, so that interferences between incident and reflected waves cannot be neglected, as a rule, in any averaged energy flow balance at boundaries; the reader is referred to previous work [Ichchou et al. (1997) for instance]. In fact, simplification rules often deal with nondissipative waveguides, with very simple propagation characteristics. Such rules cannot be considered to be general.

For the most part, uncorrelation can be interpreted using a statistical model with the following expectation hypothesis $\mathscr{E}(\mu_{I_i}^*(L)\mu_{I_j}(L)) = \delta_{ij}\mathscr{E}(|\mu_{I_i}(L)|^2)$, where $\mathscr{E}$ designates the expected value (Bocquillet, 2000). A set of new parameters denoted σ_{I_i} are thus introduced for the local energy approach derivation. Specifically, σ_{I_i} represents the contribution $\mathscr{E}(|\mu_{I_i}(L)|^2)$ to the averaged energy flow balance. Using such a model and assumptions, the incident averaged energy $\langle \Pi_I \rangle$ ($\langle \mathscr{L} \rangle$ is the local energy prediction of energy variable $\mathscr{L}$) can therefore be written as

$$\langle \Pi_I \rangle(L) = \sum_{i=1}^{n} \mathbb{P}_{i,i}\, \sigma_{I_i}(L). \tag{35}$$

Let us now define the scattered energy flow $\langle \Pi_S \rangle$ close to the boundary $z = L$. For a single incident wave μ_{I_i} at the boundary, the exact ratio between incident and reflected energy flow is supposed to be verified in the context of the local energy approach, so that

$$\frac{\langle \Pi_S \rangle}{\langle \Pi_I \rangle} \stackrel{\text{def}}{=} \frac{\Pi_S}{\Pi_I} \tag{36}$$

with

$$\frac{\Pi_S}{\Pi_I} = \frac{\mathbb{P}c_{S_{i,i}}}{\mathbb{P}c_{I_{i,i}}}, \tag{37}$$

where $\mathbb{P}c_{I_{i,i}}$ and $\mathbb{P}c_{S_{i,i}}$ are the matrix coefficients of the incident and reflected power after condensation on the incident waves, namely

$$\mathbb{P}c_I = {}^t\begin{bmatrix} \mathbb{I} \\ \mathbb{C}^{(2)} \end{bmatrix}^* \mathbb{P}_I \begin{bmatrix} \mathbb{I} \\ \mathbb{C}^{(2)} \end{bmatrix},$$

$$\mathbb{P}c_S = {}^t\begin{bmatrix} \mathbb{I} \\ \mathbb{C}^{(2)} \end{bmatrix}^* \mathbb{P}_S \begin{bmatrix} \mathbb{I} \\ \mathbb{C}^{(2)} \end{bmatrix}. \tag{38}$$

Hence, without correlation between incident waves, the reflected energy flow corresponding to n incident waves is simply the sum of all those elementary contributions. The scattered energy flow can be expressed using the local energy approach incident waves $\sigma_{I_i}(L)$ as follows:

$$\langle \Pi_S \rangle(L) \stackrel{\text{def}}{=} \sum_{i=1}^{n} \frac{\mathbb{P}c_{S_{i,i}}}{\mathbb{P}c_{I_{i,i}}} \mathbb{P}_{i,i}\, \sigma_{I_i}(L). \tag{39}$$

This definition links the reflected energy flow at the singularity to the local energy unknowns namely $\sigma_{I_i}(L)$. Let us now introduce a new set of local energy unknowns denoted below as σ_{S_j} and associated with reflected waves expectation $\mathscr{E}(|\mu_{S_j}|)^2$, so that the reflected power $\langle \Pi_S \rangle$ may be of the following form:

$$\langle \Pi_S(L) \rangle \stackrel{\text{def}}{=} -\sum_{i=1}^{n} \mathbb{P}_{n+i,n+i}\, \sigma_{S_i}(L). \tag{40}$$

Ultimately, a relationship linking the incident local energy unknowns $\sigma_{I_i}(L)$ and $\sigma_{S_i}(L)$, has to be expressed. This relationship will generalize the notion of an energy diffusion matrix, namely the matrix of reflection and transmission efficiencies.

5.5. Expressions of efficiency matrices

At the boundary $S(L)$, the efficiency matrix links vectors $\sigma_{I_i}(L)$ and $\sigma_{S_i}(L)$ as

$$\sigma_L(L) = \mathbb{E}^{(2)}\sigma_R(L). \tag{41}$$

Coefficients of this matrix are given for $(i,j = 1, \ldots, n)$ by

$$\mathbb{E}^{(2)}_{i,j} = -\frac{|\mathbb{C}^{(2)}_{i,j}|^2}{\sum_{k=1}^{n} \mathbb{P}_{n+k,n+k}|\mathbb{C}^{(2)}_{k,j}|^2} \frac{\mathbb{P}c_{S_{j,j}}}{\mathbb{P}c_{I_{j,j}}} \mathbb{P}_{j,j}. \tag{42}$$

Details of the proof and assumptions resulting in expression (42) can be found in Appendix B. It should be mentioned that the given expression incorporates a part of the coherent energy flow associated with the interference between incident and reflected waves. This contribution is often neglected in the literature (Wohlever and Bernhard, 1992; Ichchou et al., 1997). The square matrix $\mathbb{E}^{(2)}$ is the energy diffusion matrix at section $S(L)$. In practice, $\mathbb{E}^{(2)}$ groups the reflection and transmission efficiencies associated with the propagation waves at section $S(L)$. This definition of efficiency matrix ensures that at conservative discontinuities the energy flow vanishes. In the case of nonconservative boundaries, the intended sign of total energy flow will be respected.

For the boundary $z = 0$ (see Fig. 6), a similar relation can be found, with the adjunction of an excitation term $\boldsymbol{\sigma}_{ex}$:

$$\sigma_R(0) = \mathbb{E}^{(1)}\sigma_L(0) + \sigma_{ex}, \tag{43}$$

This expression comes from similar uncorrelation assumptions. Where σ_{ex} is the contribution of external sources. These quantities have to be specified.

5.6. Injected power distribution

The main concern here is to define how injected power can be shared among different waves. Similarly, the part of this injected power affecting each wave have to be defined. In practice, the injected power $\Pi_{\text{inj}} = \Pi(0)$ can be split into five terms:

$$\Pi_{\text{inj}} = \Pi_{\text{inf}} + \Pi_I(0) - \Pi_S(0) + \Pi_{ex,I}(0) + \Pi_{ex,S}(0), \tag{44}$$

where Π_{inf} denotes the injected power when the duct is semi-infinite, considering incident waves only. The terms $\Pi_I(0)$ and $\Pi_S(0)$ represent the incident and reflected energy flow due to the incident waves coming from the opposite boundary. Here, $\Pi_{ex,I}, \Pi_{ex,S}$ are the contribution of interferences between excitation and incident-reflected waves. As the excitation can be viewed as a source of waves, uncorrelated with the incident waves μ_{L_j}, the assumption $\mathscr{E}(\mu^*_{L_i}(0)\mu_{ex_j}) = 0$ can be used. As this singularity is conservative, the local energy approach power balance on the first boundary may be written as

$$\langle \Pi_{\text{inj}} \rangle = \Pi_{\text{inf}} + \langle \Pi_I(0) \rangle - \langle \Pi_S(0) \rangle = \Pi_{\text{inf}}. \tag{45}$$

In this case, the injected power is that of the semi-infinite pipe. Also, the source contributes in an independent manner to the energy flow going out of the singularity. As the propagation tends to uncorrelate the waves, the injected energy flow can be asymptotically distributed on the out-going waves:

$$\mathbb{P}_{i,i}\sigma_{ex_i} \overset{\text{hyp}}{=} \frac{\mathbb{P}_{i,i}|\mu_{ex_i}|^2}{\sum_{k=1}^{n} \mathbb{P}_{S_{n+k,n+k}}|\mu_{ex_k}|^2}\Pi_{\text{inf}} = \mathbb{P}_{i,i}r_{ex_i}\Pi_{\text{inf}}. \tag{46}$$

Henceforth, vector σ_{ex} introduced in the local energy modelling, will be given by

$$\sigma_{ex_i} \overset{\text{def}}{=} \frac{|\mu_{ex_i}|^2}{\sum_{k=1}^{n} \mathbb{P}_{S_{n+k,n+k}}|\mu_{ex_k}|^2}\Pi_{\text{inf}} = r_{ex_i}\Pi_{\text{inf}}. \tag{47}$$

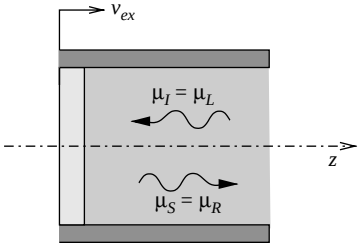

Fig. 6. Scattering of propagation modes μ_{L_j} on the boundary $S(0)$.

This vector is directly associated to the kinematic wave input vector μ_{ex}. The wave input energy ratio vector r_{ex} is then given by

$$r_{ex_i} = \frac{|\mu_{ex_i}|^2}{\sum_{k=1}^{n} \mathbb{P}_{S_{n+k,n+k}} |\mu_{ex_k}|^2}. \tag{48}$$

Eqs. (41) and (43) define the required expressions for the local energy model resolution.

5.7. Energy balance far from singularities—local energy system equations

To conclude the energy analysis, some basic transfer expressions linking the local energy unknowns, i.e., σ_R and σ_L, are given. This is done thanks to an energy flow balance far from singularities. We recall the general wave transport given earlier in this paper, i.e.,

$$\mu(z') = \mathbb{D}(z' - z)\mu(z). \tag{49}$$

It can easily be shown, by using similar energy balances and uncorrelation hypothesis used before, that

$$\sigma(z') = \mathbb{D}(z' - z)\mathbb{D}^*(z' - z)\sigma(z). \tag{50}$$

In fact, no interferences are used in the local energy model construction far from singularities. This expression leads asymptotically to

$$\sigma(L) = \mathbb{D}(L)\mathbb{D}^*(L)\sigma(0) = \mathbb{F}\,\sigma(0). \tag{51}$$

Ultimately, the system of resolution for the local energy approach unknown (namely $\underline{\sigma}$) can be constructed with Eqs. (B.9), (43) and (51). It may be written as

$$\mathbb{S}\begin{bmatrix} \sigma_L(0) \\ \sigma_R(L) \end{bmatrix} = \begin{bmatrix} \sigma_{ex} \\ 0 \end{bmatrix}, \tag{52}$$

where matrix $\mathbb{S}$ is

$$\mathbb{S} = \begin{bmatrix} -\mathbb{E}^{(1)} & \mathbb{F}^{-1} \\ -\mathbb{I} & \mathbb{F}^{-1}\mathbb{E}^{(2)} \end{bmatrix}. \tag{53}$$

Numerical inversion of system (52) leads to the boundary local energy unknowns. These boundary parameters enable the determination of related unknowns far from singularities using relationship (50). Those quantities are ultimately used for the reconstruction of averaged energy flow as well as kinetic and potential energy densities.

5.8. Reconstruction of averaged energy fields

Once system (52) is solved, the reconstruction of energy flow at any section of the waveguide is thorough. The bilinear forms of the kinetic and potential energy on the sections can be determined by using the matrixes of the differential system. Hence, away from boundaries, the simplified model will give smooth energy levels with the following expressions:

$$\langle \Pi \rangle(z) = \sum_{j=1}^{2n} \mathbb{P}_{i,i}\sigma_j(z),$$

$$\langle U_p \rangle(z) = \sum_{j=1}^{2n} \mathbb{K}_{\mu_{j,j}}\sigma_j(z),$$

$$\langle T_k \rangle(z) = \sum_{j=1}^{2n} \mathbb{M}_{\mu_{j,j}}\sigma_j(z). \tag{54}$$

For a section which is close to a boundary, some coherent contribution will be added. Thus, the following expressions are used close to the section boundary $S(L)$:

$$\langle \Pi \rangle(z) = \sum_{j=1}^{n} \mathbb{P}c_{j,j}\sigma_{I_j}(z),$$

$$\langle U_p \rangle(z) = \sum_{j=1}^{n} \mathbb{K}c_{\mu_{j,j}}\sigma_{I_j}(z),$$

$$\langle T_k \rangle(z) = \sum_{j=1}^{n} \mathbb{M}c_{\mu_{j,j}}\sigma_{I_j}(z); \tag{55}$$

matrixes $\mathbb{P}c$, $\mathbb{K}c_\mu$ and $\mathbb{M}c_\mu$ are defined as follows:

$$\mathbb{M}c_\mu(z) = {}^t\begin{bmatrix} \mathbb{I} \\ \mathbb{C}^{(2)}(z) \end{bmatrix}^* \mathbb{M}_\mu(z) \begin{bmatrix} \mathbb{I} \\ \mathbb{C}^{(2)}(z) \end{bmatrix},$$

$$\mathbb{K}c_\mu(z) = {}^t\begin{bmatrix} \mathbb{I} \\ \mathbb{C}^{(2)}(z) \end{bmatrix}^* \mathbb{K}_\mu(z) \begin{bmatrix} \mathbb{I} \\ \mathbb{C}^{(2)}(z) \end{bmatrix}. \tag{56}$$

It should be mentioned that expressions (54) and (55) give exactly the same prediction of energy fields close to boundaries.

6. Results and comments

The example proposed above is considered here. Table 1 summarizes the parameters used. The absorber characteristics are as follows: the mass of the piston, the dissipation and the nondimensional natural frequency are, respectively, $M = \pi a^2 L/100$, $\xi = 0.05$, $\varpi_m = 0.28$. A computation involving the propagating modes was first

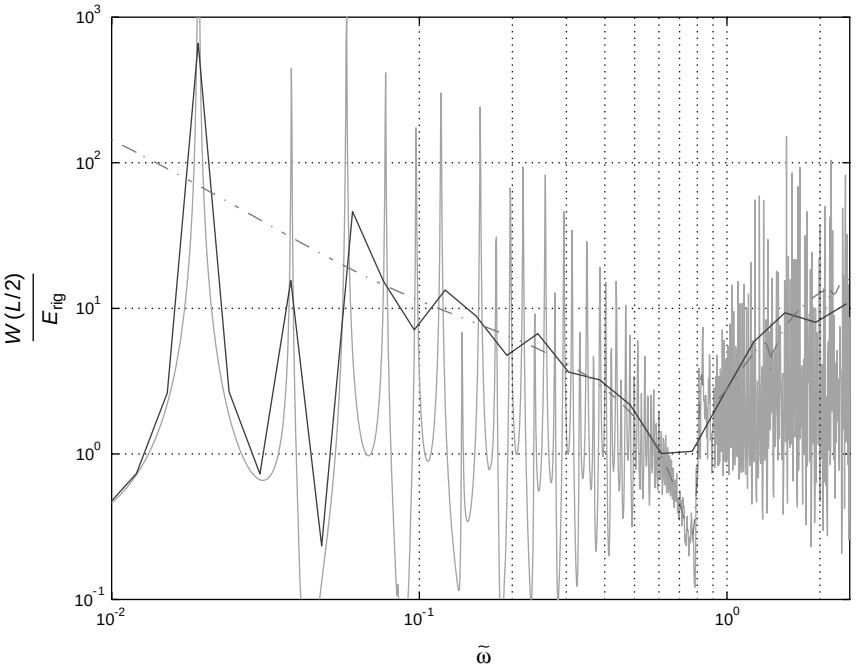

Fig. 7. Comparison between the energy model presented here and exact calculation. Normalized total energy density at the section $z = L/2$ of the pipe: (....), exact computation; (—), 1/3 octave band result; (- · -), present method.

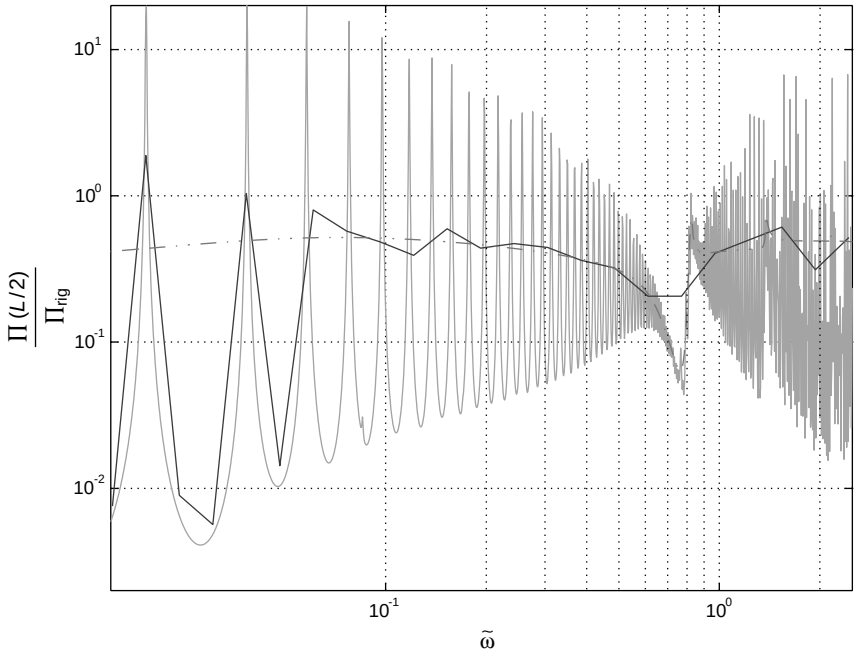

Fig. 8. Comparison between the energy model presented here and exact calculation. Normalized energy flow at the section $z = L/2$ of the pipe: (....), exact computation; (—), 1/3 octave band result; (- · -), present method.

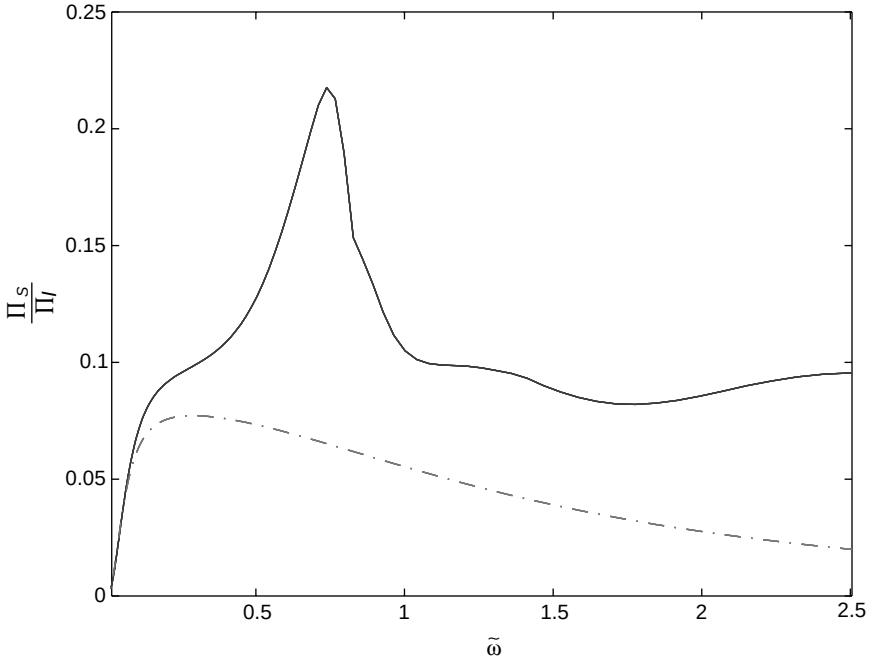

Fig. 9. Reflection efficiency of boundary $z = L$ for: (- · -) a rigid pipe; (—) a flexible pipe.

performed. It allowed calculation of energy densities and energy flow without any simplification. This computation provides reference results for validations of the local energy approach. Using the developments given above, the local energy approach model of the fluid-filled pipe was performed.

Fig. 7 gives a comparison between the two computations on the section located at the middle of the pipe. The ratio of the computed total energy density to the total energy density corresponding to a rigid semi-infinite pipe (referred to by

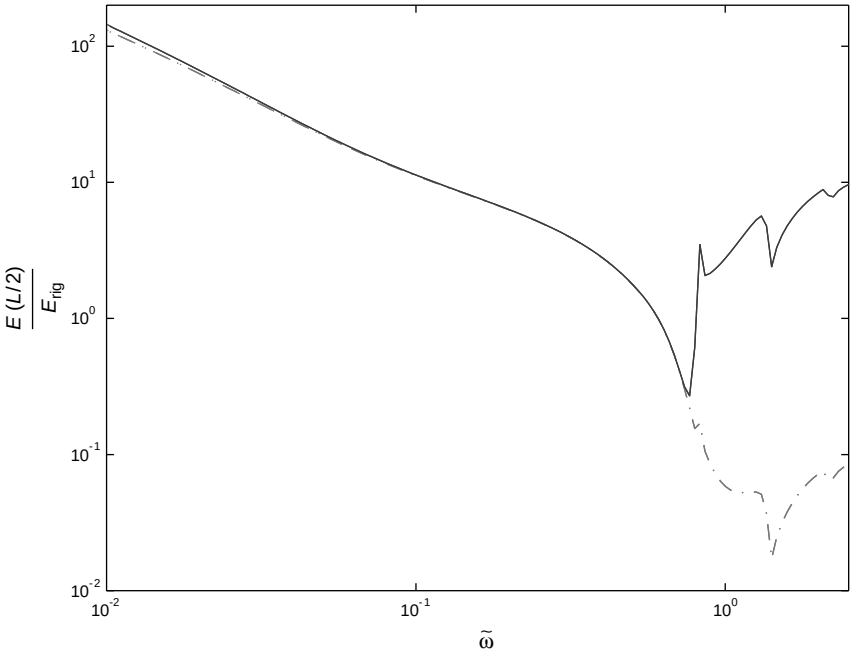

Fig. 10. Contribution of: (- · -), wave (1) and (—), waves (1,2) to total energy on section $z = L/2$ for the present energy model.

E_{rig}) is first plotted. This figure includes a 1/3 octave calculation of the "exact" energy levels and shows satisfactory agreement with the local energy approach prediction. Stiff variations are observed at cut-on frequencies of propagating modes (3) and (4). In addition, around $\varpi = 0.8$, the first two propagating modes change nature (Fuller and Fahy, 1982) involving frequency variations in the repartition of energy between propagating modes.

Fig. 8 gives a comparison of the kinematic ratio of the computed energy flow at $S(L/2)$ to the energy flow corresponding to a rigid semi-infinite pipe (referred to by Π_{rig}). Comparisons of local energy approach predictions concur with the 1/3 octave "exact" calculation. This agreement validates the assumptions given in the previous section. In fact, the local energy approach provides at each point of the system an averaged value of energy quantities.

Fig. 9 presents the energy transmission of the wave (1) to the piston/spring–damper system, for the studied and rigid pipe cases. In the case of the rigid pipe, the maximum of absorbed power corresponds to the natural frequency of the piston; the fluid structure coupling especially modifies the interaction between the first wave and the one degree of freedom system when the frequency increases.

The result presented in Fig. 10 addresses the propagating complexity role within the context of local energy approach computation. In this figure, the local energy approach results can be compared when several propagating modes contributes to the response. In low frequencies, the propagating mode (1), which is very close to the plane acoustical wave, contributes preponderantly to the dynamics of the pipe, as it is easily excited at the boundary $S(z = 0)$.

At frequencies over $\varpi = 0.8$, this wave changes in nature (the energy is predominant in the structure), and the second wave, becoming a "fluid wave", holds the majority of energy in the section. *This clearly shows that very poor predictions are obtained when a single propagating mode is used to formulate local energy approach computations. This result confirms the interest of the proposed propagating approach for high-frequency modelling of the dynamics.*

7. Concluding remarks

In this paper, the formulation and generalization of a propagating approach to elastoacoustic problems have been presented. This is a powerful tool for the computation of dispersion relations. This approach can also be implemented under a finite element code in order to deal with complex elastoacoustic cases. The mixed variable description in conjunction with the state-space formulation used, leads to a well-posed spectral problem. The solution of the latter defines a set of orthogonal propagating vectors. This is a new basis of the dynamical motion, namely forces and

velocities. Resolution of the kinematic case is then formulated in terms of wave properties rather than the classical forces/velocities considerations.

The energy parameters, namely the kinetic energy density, potential energy density and the active energy flow were formulated using the new wave basis. These expressions clearly show the energy parameter properties and provide a comprehensive way for their simplification. In fact, the wave interference contribution to the energy is clearly related to the off-diagonal terms in the associated energy matrix. A number of explanations were given in order to interpret the concept of "destructive interferences". Hence, assuming uncorrelated waves far from singularities, this leads to a quadratic superposition principle and leads to a new energy-unknown problem to be formulated. The energy unknowns correspond to the wave amplitude value. No phase considerations are taken into account here. This problem constitutes the basis of the local energy approach. Analysis of the energy boundary properties makes it possible to close the posed energy problem.

The application to a fluid-filled pipe shows the *propagating complexity* of the dynamics when frequency increases. The propagation approach provides a relevant description of the statistical analysis of power transfer. The propagating modes are used as a set of input data in view of the definition of the local energy approach as well as the SEA. The fluid-filled pipe system given in this paper is just an illustration of the general procedure developed for complex waveguides. Further applications showing the interest of the presented approach will be reported.

Acknowledgements

Part of the research presented here is based on a contract with Electricity of France. The authors gratefully acknowledge them (EDF/DER, Paris) for their support and Miss R. Reynaud for assistance with English. Thanks also to reviewers and editors for their contributions.

Appendix A. Some vectors and matrix definitions

Let us define $\mathbf{u}^{(s)}$ and $\mathbf{f}^{(s)}$ representing the components of the kinematic behavior (displacements as well as forces and moments) for the Donnell–Mushtari shell theory:

$$\mathbf{u}^{(s)} = \begin{bmatrix} u_z \\ w \\ \phi \end{bmatrix} \quad \text{and} \quad \mathbf{f}^{(s)} = \begin{bmatrix} N_z \\ -T \\ M_z \end{bmatrix}. \tag{A.1}$$

With those parameters in mind, the state-space vector is found to be simply

$$\mathbf{Y}^{(s)} = \begin{bmatrix} u \\ w \\ \phi \\ N_z \\ -T \\ M_z \end{bmatrix}. \tag{A.2}$$

The state-space matrix associated with the state-space vector given below and to the structural model adopted in this study is thus shown to be

$$\mathbb{H}^{(s)} = \begin{bmatrix} \rho h\omega^2 & 0 & 0 & 0 & 0 & 0 \\ 0 & \dfrac{h(-E+\rho\omega^2 a^2)}{a^2} & 0 & -\dfrac{\nu}{a} & 0 & 0 \\ 0 & 0 & 0 & 0 & 1 & 0 \\ 0 & -\dfrac{\nu}{a} & 0 & \dfrac{1}{C} & 0 & 0 \\ 0 & 0 & 1 & 0 & 0 & 0 \\ 0 & 0 & 0 & 0 & 0 & \dfrac{1}{D} \end{bmatrix}. \tag{A.3}$$

Variables C and D are given in the main text. Finally, the matrix $\mathbb{J}_a^{(s)}$ is given by

$$\mathbb{J}_a^{(s)} = \begin{pmatrix} \mathbb{O}_3 & -\mathbb{I}_3 \\ \mathbb{I}_3 & \mathbb{O}_3 \end{pmatrix}. \tag{A.4}$$

For the coupled elastoacoustic case, the coupled state-space vector has the following expression:

$$\mathbf{Y}^{(c)} = \begin{bmatrix} \mathbf{p} \\ u \\ w \\ \phi \\ f^{(a)} = \dfrac{1}{\rho_f \omega^2} \underline{\mathbf{M}}^{(a)} \dfrac{\mathrm{d}\mathbf{p}}{\mathrm{d}z} \\ 2\pi a N_z \\ -2\pi a T \\ 2\pi a M_z \end{bmatrix}. \tag{A.5}$$

Here, $\mathbf{p} = (p_j)_{j=1,m}$ and $\mathrm{d}\mathbf{p}/\mathrm{d}z = (\mathrm{d}p/\mathrm{d}z)_{j=1,m}$. So that the state-space matrix associated with the interpolation functions proposed in the main text becomes

$$\mathbb{H}^{(c)} = \begin{bmatrix} \dfrac{1}{\rho\omega^2}\mathbb{K}^{(a)} & {}^t\mathbb{B} & \mathbb{O} & \mathbb{O} \\ \mathbb{B} & \mathbb{K}^{(s)} & \mathbb{O} & \mathbb{Q}^{(s)} \\ \mathbb{O} & \mathbb{O} & \rho\omega^2\mathbb{M}^{(a)} & \mathbb{O} \\ \mathbb{O} & {}^t\mathbb{Q}^{(s)} & \mathbb{O} & \mathbb{M}^{(s)} \end{bmatrix}; \tag{A.6}$$

matrixes $\mathbb{J}_a^{(c)}$, $\mathbb{B}$, $\mathbb{M}^{(s)}$, $\mathbb{K}^{(s)}$ and $\mathbb{Q}^{(s)}$ are, respectively, given by

$$\mathbb{J}_a^{(c)} = \begin{bmatrix} \mathbb{O}_n & -\mathbb{I}_n \\ \mathbb{I}_n & \mathbb{O}_n \end{bmatrix}, \quad \mathbb{B} = 2\sqrt{\pi}\, a \begin{bmatrix} 0 & \dots & 0 \\ 1 & \dots & 1 \\ 0 & \dots & 0 \end{bmatrix},$$

$$\mathbb{M}^{(s)} = \frac{1}{2\pi a} \begin{bmatrix} 1/C & 0 & 0 \\ 0 & 0 & 0 \\ 0 & 0 & 1/D \end{bmatrix}, \tag{A.7}$$

and:

$$\mathbb{K}^{(s)} = 2\pi a \begin{bmatrix} \rho h \omega^2 & 0 & 0 \\ 0 & \dfrac{h(-E + \rho\omega^2 a^2)}{a^2} & 0 \\ 0 & 0 & 0 \end{bmatrix},$$

$$\mathbb{Q}^{(s)} = \begin{bmatrix} 0 & 0 & 0 \\ -\dfrac{v}{a} & 0 & 0 \\ 0 & 1 & 0 \end{bmatrix}. \tag{A.8}$$

Finally, diagonal matrixes $\mathbb{M}^{(a)}$ and $\mathbb{K}^{(a)}$ introduced in the state-space expression of the coupled elastoacoustic problem, are

$$M_{j,j}^{(a)} = \frac{1}{a^2}, \quad K_{j,j}^{(a)} = (a^2 * \mathbf{k}^2 - \vartheta_j^2), \tag{A.9}$$

where ϑ_j designates the jth root of the Bessel function of the first kind, and with $\mathbf{k} = \omega/c$ a real value, c being the fluid-specific velocity.

Appendix B. Efficiency matrix derivation

In this appendix, the expression of the efficiency matrix $\mathbb{E}^{(2)}$ is derived. The efficiency matrix $\mathbb{E}^{(1)}$ associated with the boundary $S(0)$ can be reached using quite a similar demonstration. Let us consider the case of a unique incident wave μ_{I_i}. The reflected waves μ_S tend to uncorrelate themselves away from the singularity. Thus, it can asymptotically ($z \to L$) be established that the mean value of reflected energy, initially expressed in terms of reflected waves (33) can be derived under the following form:

$$\mathscr{E}(\Pi_S(z)) = -\sum_{j=1}^{n} \mathbb{P}_{n+j,n+j}\mathscr{E}(|\mu_{S_j}(z)|)^2. \tag{B.1}$$

Using expression (26) defining the wave kinematic diffusion matrix at the boundary ($z = L$), the previous equation becomes

$$\mathscr{E}(\Pi_S(z)) = -\left[\sum_{j=1}^{n} \mathbb{P}_{n+j,n+j}|\mathbb{C}^{(2)}_{j,i}\lambda_j(L-z)|^2\right] \mathscr{E}(|\mu_{I_i}(L)|^2). \tag{B.2}$$

Finally, when ($z \to L$), the reflected energy flow associated with the unique incident wave μ_{I_i}, can be shown to be approximately

$$\mathscr{E}(\Pi_S(z)) \approx -\left[\sum_{j=1}^{n} \mathbb{P}_{n+j,n+j}|C^{(2)}_{j,i}|^2\right]\mathscr{E}(|\mu_{I_i}(L)|^2). \tag{B.3}$$

Expression (B.3) specifies the distribution of reflected energy on the reflected waves for the local energy model. In fact, the part of reflected uncorrelated energy associated with the incident wave μ_{I_j} can be defined by

$$-\frac{\mathbb{P}_{n+j,n+j}\mathscr{E}(|\mu_{L_j}(z)|^2)}{\mathscr{E}(\Pi^{(2)}_S(z))} \overset{\text{def}}{\approx} \frac{\mathbb{P}_{n+j,n+j}|\mathbb{C}^{(2)}_{j,i}|^2}{\sum_{k=1}^{n}\mathbb{P}_{n+k,n+k}|\mathbb{C}^{(2)}_{k,i}|^2}. \tag{B.4}$$

Let us assume, in the context of the simplified local energy model, that the reflected energy flow $\langle \Pi^{(2)}_S(L)\rangle$ will respect similar wave distribution to the one given in Eq. (B.4) on reflected waves σ_{L_j}:

$$-\mathbb{P}_{n+j,n+j}\sigma_{S_j}(L) \overset{\text{hyp}}{=} \frac{\mathbb{P}_{n+j,n+j}|\mathbb{C}^{(2)}_{j,i}|^2}{\sum_{k=1}^{n}\mathbb{P}_{n+k,n+k}|\mathbb{C}^{(2)}_{k,i}|^2}\langle \Pi_S\rangle(L); \tag{B.5}$$

$\mathbb{P}_{n+j,n+j}\sigma_{S_j}$ represents the part of reflected energy due to the incident wave μ_{I_i} and which is transported by the reflected propagation mode μ_{S_j}. Reflected energy unknowns $\sigma_{S_j}(L)$ are thus linked to the incident variables $\sigma_{I_i}(L)$ thanks to Eq. (B.6), and to Eq. (B.5), so that

$$\langle \Pi_S\rangle(L) = \frac{\mathbb{P}c_{S_{i,i}}}{\mathbb{P}c_{I_{i,i}}}\mathbb{P}_{i,i}\,\sigma_{I_i}(L); \tag{B.6}$$

and thus, in regard to expression (B.5),

$$-\mathbb{P}_{n+j,n+j}\sigma_{S_j}(L) = \frac{\mathbb{P}_{n+j,n+j}|\mathbb{C}^{(2)}_{j,i}|^2}{\sum_{k=1}^{n}\mathbb{P}_{n+k,n+k}|\mathbb{C}^{(2)}_{k,i}|^2}\frac{\mathbb{P}c_{S_{i,i}}}{\mathbb{P}c_{I_{i,i}}}\mathbb{P}_{i,i}\sigma_{I_i}(L). \tag{B.7}$$

Moreover, each incident wave contributes independently to the net reflected energy flow, the latter will readily be given by the sum of all the contributions (i). Hence,

$$\sigma_{S_j}(L) = -\sum_{i=1}^{n}\frac{|\mathbb{C}^{(2)}_{j,i}|^2}{\sum_{k=1}^{n}\mathbb{P}_{n+k,n+k}|\mathbb{C}^{(2)}_{k,i}|^2}\frac{\mathbb{P}c_{S_{i,i}}}{\mathbb{P}c_{I_{i,i}}}\mathbb{P}_{i,i}\sigma_{I_i}(L). \tag{B.8}$$

In the introduced sum (B.8), one can distinguish two main ratio contributions. The first ratio traduces the distribution of reflected net energy flow on the scattering waves μ_S from the singularity. The second ratio, traduces assumption (B.5) expressing the energy balance $\Pi^{(2)}_S/\Pi^{(2)}_I$ for each incident propagating mode. Finally, let us introduce the relationship

combining incident and reflected parameters, namely $\sigma_I(L)$ and $\sigma_S(L)$, such that

$$\sigma_S(L) = \mathbb{E}^{(2)}\sigma_I(L), \tag{B.9}$$

which is equivalent to (see Fig. 5)

$$\sigma_L(L) = \mathbb{E}^{(2)}\sigma_R(L). \tag{B.10}$$

Coefficients of this matrix are given, for $(i,j = 1, \ldots, n)$, by

$$\mathbb{E}^{(2)}_{i,j} = -\frac{|\mathbb{C}^{(2)}_{i,j}|^2}{\sum_{k=1}^{n} \mathbb{P}_{n+k,n+k}|\mathbb{C}^{(2)}_{k,j}|^2} \frac{\mathbb{P}_{c_{S_{j,j}}}}{\mathbb{P}_{c_{I_{j,j}}}} \mathbb{P}_{j,j}. \tag{B.11}$$

This is a square matrix grouping the reflection coefficients. These efficiency matrixes make it possible to close the local energy problem.

References

Belov, V.D., Rybak, S.A., Tartakovskii, B.D., 1977. Propagation of vibrational energy in absorbing structures. Soviet Physics and Acoustics 23, 115–119.

Bocquillet, A., 2000. Méthode énergétique de caractérisations vibroacoustiques des réseaux complexes. Ph.D. Thesis, Ecole Centrale de Lyon, 00-01.

Bouthier, O.M., Bernhard, R.J., 1995a. Simple models of energy flow in vibrating membranes. Journal of Sound and Vibration 182, 129–147.

Bouthier, O.M., Bernhard, R.J., 1995b. Simple models of energy flow in vibrating plates. Journal of Sound and Vibration 182, 149–164.

Carcaterra, A., Sestieri, A., 1995. Energy density equations and power flow in structures. Journal of Sound and Vibration 188, 269–282.

Dhatt, G., Batoz, J.L., 1992. Modélisation des structures par éléments finis. Hermes, Paris.

Fahy, F.J., 1994. Statistical energy analysis: a critical overview. Philosophical Transactions of the Royal Society of London A 346, 431–447.

Finnveden, S., 1997a. Formulas for modal density and for input power for mechanical and fluid point sources in fluid filled pipes. Journal of Sound and Vibration 208, 705–728.

Finnveden, S., 1997b. Spectral finite element analysis of the vibration of straight fluid-filled pipes with flanges. Journal of Sound and Vibration 199, 125–154.

Fuller, C.R., Fahy, F.J., 1982. Characteristics of wave propagation and energy distributions in cylindrical elastic shells filled with fluid. Journal of Sound and Vibration 81, 501–518.

Heckl, M., 1962. Vibrations of point driven cylindrical shell. Journal of the Acoustical Society of America 34, 1553–1557.

Houillon, L., 1999. Modélisation vibratoires des carrosseries automobiles en moyennes et hautes fréquences. Ph.D. Thesis, Ecole Centrale de Lyon, 99–49.

Ichchou, M.N., Jezequel, L., 1996. Comments on simple models of the energy flow in vibrating membranes and transversely vibrating plates. Journal of Sound and Vibration 195, 679–685.

Ichchou, M.N., Lebot, A., Jezequel, L., 1997. Energy models of one-dimensional multi-propagative systems. Journal of Sound and Vibration 201, 535–554.

Keane, A.J., Price, W.G., 1997. Statistical Energy Analysis: An Overview with Applications. Cambridge University Press, Cambridge.

Kumar, R., 1972. Dispersion of axially symmetric waves in empty and fluid-filled cylindrical shells. Acoustica 27, 317–329.

Kumar, R., Stephens, R.W., 1972. Dispersion of flexural waves in circular cylindrical shells. Proceedings of the Royal Society of London A 329, 283–297.

Langley, R.S., 1994a. The modal density and mode count of thin cylinders and curved panels. Journal of Sound and Vibration 169, 43–53.

Langley, R.S., 1994b. Wave motion and energy flow in cylindrical shells. Journal of Sound and Vibration 169, 29–42.

Langley, R.S., 1995. On the vibrational conductivity approach to high-frequency dynamics for two-dimensional structures components. Journal of Sound and Vibration 182, 637–657.

Lase, Y., Ichchou, M.N., Jezequel, L., 1996. Energy analysis of bars and beams: theoretical formulations. Journal of Sound and Vibration 192, 281–305.

Lyon, R.H., 1975. Statistical Energy Analysis of Dynamical Systems. MIT Press, Cambridge.

Markus, S., 1988. The Mechanics of Vibrations of Cylindrical Shells. Elsevier, Amsterdam.

Mead, D.J., 1973. A general theory of harmonic wave propagation in linear periodic systems with multiple coupling. Journal of Sound and Vibration 27, 235–260.

Miller, D.W., Von Flotow, A., 1989. A travelling wave approach to power flow in structural networks. Journal of Sound and Vibration 128, 145–162.

Nefske, D.J., Sung, S.H., 1987. Power flow finite element analysis of dynamic systems: basic theory and application to beams. NCA Publication 3, 47–54.

Orenius, U., Finnveden, S., 1996. Calculation of wave propagation in rib-stiffened plate structures. Journal of Sound and Vibration 198, 203–224.

Pavic, G., 1990. Vibrational energy flow in elastic circular cylindrical shells. Journal of Sound and Vibration 142, 293–310.

Pease, M.C., 1978. Methods of Matrix Algebra. Academic Press, New York, London.

Sinha, B.K., Plona, T.J., Kotec, S., Chang, S., 1992. Axisymmetric wave propagation in fluid-loaded cylindrical shells: (i) theory. Journal of the Acoustical Society of America 92, 1132–1143.

Wang, Z., Norris, A.N., 1995. Wave in cylindrical shells with circonferential submenbers: a matrix approach. Journal of Sound and Vibration 181, 457–484.

Wohlever, J.C., Bernhard, R.J., 1992. Mechanical energy flow models of rods and beams. Journal of Sound and Vibration 153, 1–19.

Yakubovitch, V.A., Starzhinskii, V.M., 1975. Linear Differential Equations with Periodic Coefficients. Halsted Press, New York.

Yong, Y., Lin, Y.K., 1989. Propagation of decaying waves in periodic and piecewise structures of finite length. Journal of Sound and Vibration 129, 99–118.